Applied Remote Sensing

Remote Sensing. SPIE Digital Library. org

Bistatic antenna configurations for air-launched ground penetrating radar

Daniel Orfeo Yu Zhang Dylan Burns Jonathan Miller Dryver Huston Tian Xia



Bistatic antenna configurations for air-launched ground penetrating radar

Daniel Orfeo, Yu Zhang, Dylan Burns, Jonathan Miller, b Dryver Huston,^{a,*} and Tian Xia^a

^aUniversity of Vermont, School of Engineering, Burlington, Vermont, United States ^bWhite River Technologies, Inc., Lebanon, New Hampshire, United States

Abstract. Ground penetrating radar (GPR) is valuable for the detection of subsurface objects with little or no metal content, such as plastics, ceramics, and concrete piping. However, the effects of antenna configuration parameters, such as height and angle, are not well studied for all sensing applications. GPR simulations and laboratory GPR experiments are performed to evaluate the effects of antenna angle and height on the sensitivity of bistatic air-launched GPR, to search for buried nonmetallic objects. The results presented provide guidance for the development of air-launched GPR systems installed on unmanned aerial vehicles for in-flight subsurface scanning of buried targets. © 2019 Society of Photo-Optical Instrumentation Engineers (SPIE) [DOI: 10 .1117/1.JRS.13.027501]

Keywords: ground penetrating radar; air-launched; bistatic; buried object; nonmetallic; unmanned aerial vehicle.

Paper 180878 received Oct. 31, 2018; accepted for publication Mar. 28, 2019; published online Apr. 23, 2019.

1 Introduction

There is an urgent and longstanding need for noncontact subsurface imaging for the detection and identification of buried objects. 1,2 Ground penetrating radar (GPR) has been proved to be an effective system for detecting objects with little to no metal content, such as plastic, ceramic, and concrete pipes.^{3–8} These nonmetallic objects often have dielectric properties similar to those of their burial media, necessitating a high degree of detection sensitivity. One possible means to increase detection sensitivity is to use multiple antennae. 10 A bistatic radar is a common configuration with one transmitter and one receiver that are not colocated. 11 Based on the mounting positions of the antennae, GPR systems can be classified into two categories: ground-coupled GPR or air-launched GPR. Ground-coupled GPR systems have antennae installed closer to the detection surface, which results in small signal loss and high detection sensitivity. In airlaunched GPR systems, antennae are typically operated at heights greater than one-quarter of the operating wavelength. Compared to ground-coupled GPR, the use of air-launched GPR provides the convenience of contactless survey on a large area in a short period of time. 12,13

In both categories, the antenna setting parameters—including antenna height and angle play vital roles in determining GPR sensing performance. Much of the current body of GPR research involves traditional ground-coupled systems. For example, Kang et al. 14 considered the placement of ground-coupled bistatic antennae for the detection of subsurface cavities, and in a subsequent study, the impact of antenna height on data quality when searching for buried objects is considered.¹⁵ However, these studies do not include simultaneous variation of antenna angle, nor do they treat antenna heights greater than 20 cm above the ground surface. Bloemenkamp and Slob 16 used a bistatic 900 MHz time-domain GPR at antenna heights between 0 and 20 cm to conclude that signal quality deteriorates more rapidly for vertical two-way signal travel distances greater than one-third of the dominant wavelength. It is not addressed whether this relationship will hold for a step-frequency GPR, which sweeps through a larger frequency range. An understanding of the effects of these parameters—including simultaneous variation of

1931-3195/2019/\$25.00 © 2019 SPIE

^{*}Address all correspondence to Dryver Huston, E-mail: dryver.huston@uvm.edu

antenna angle and height, with heights on the order of 1 m—is of importance for the design of a UAV-mounted GPR system. In this study, several realistic antenna configurations for frequency-domain air-launched GPR are tested. Experimental setups are designed with consideration for a bistatic system with transmitter and receiver antennae mounted on separate UAVs.

2 Air-Launched GPR Theory

To reach a target, a transmitted signal must penetrate through various media and across media interfaces, as shown in Fig. 1. In this paper, a simple experimental setup is considered in which a single target is buried in sand. Diffuse scattering is not a major issue in such an uncluttered test environment. In a complex scenario with more scattering, a surface-clutter removal algorithm could be used.

The dielectric constants of the media determine how much of a signal reflects and how much continues to penetrate. In the special case where the angle of incidence θ_i equals 0 deg, the reflection coefficient between two media, R_{12} , is the ratio of the amplitudes of the reflected signal S_2 and the incident signal S_1 , ¹⁷ whose value is determined

$$R_{12} = \frac{\sqrt{\varepsilon_1} - \sqrt{\varepsilon_2}}{\sqrt{\varepsilon_1} + \sqrt{\varepsilon_2}} = \frac{n_2 - n_1}{n_1 + n_2},\tag{1}$$

where ε_1 and ε_2 are the respective dielectric constants of the two media, and n_1 and n_2 are the indices of refraction of the two media. For a given media interface, the portion of the signal that reflects or penetrates is fixed with respect to other antenna parameters. Therefore, a measure of the strength of the reflected signal S_2 can be used to calculate the strength of the penetrating signal, S_3 . The quality of a GPR subsurface survey improves as the strength of the penetrating signal increases. For the general case of transverse electric (TE)-polarized waves with a nonzero angle of incidence, the reflection coefficient 17 is calculated:

$$R_{\text{TE}} = \frac{n_1 \cos \theta_i - n_2 \cos \theta_t}{n_1 \cos \theta_i + n_2 \cos \theta_t}.$$
 (2)

For the alternate case of transverse magnetic (TM) polarized waves, the general reflection coefficient is calculated:

$$R_{\text{TM}} = \frac{n_2 \cos \theta_i - n_1 \cos \theta_t}{n_1 \cos \theta_t + n_2 \cos \theta_i}.$$
 (3)

A comparison of R_{TE} and R_{TM} reveals that it is possible for the reflection to vanish only in the case of TM polarization.¹⁷ The angle of incidence at which this occurs is the Brewster's angle:

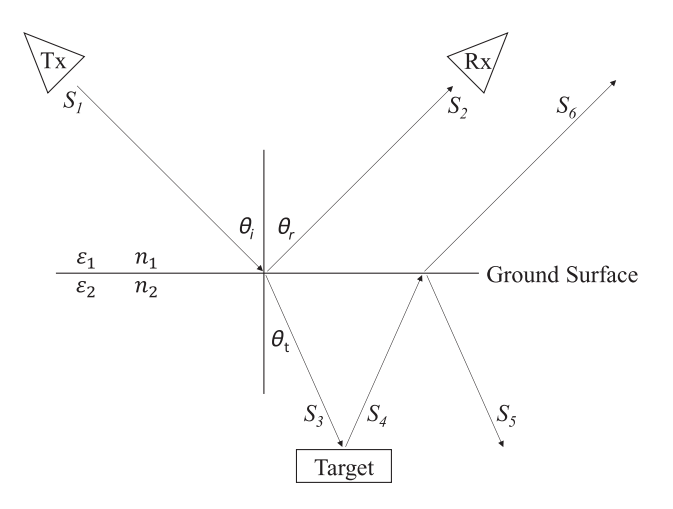


Fig. 1 Signal reflection and penetration across media boundary.

$$\theta_r + \theta_t = \frac{\pi}{2}.\tag{4}$$

At the Brewster's angle, the reflected signal S_2 vanishes, making determination of the penetrating signal, S_3 , impossible. To avoid this limitation of TM polarization, TE polarization is chosen for the GPR experiments discussed in this paper.

3 Simulation Study

3.1 Simulation Setup

Simulations using the radar modeling program gprMax were performed to investigate the impact of antenna mounting height on GPR sensitivity, as shown in Fig. 2. The gprMax program uses the finite-difference time-domain method to simulate electromagnetic wave propagation for modeling GPR. ¹⁸ It was chosen for its high accuracy and generous GNU General Public License.

Simulations of antenna angles were not possible as the gprMax program considers antennae to be isotropic radiators. Modeling the antennae as isotropic radiators is not a limitation for simulating antenna heights. Without clutter or secondary targets, there are no multipath effects in these simulations, so omnidirectional antennae will produce the same results as nonisotropic antennae, which have the same directional gain in the direction of interest. The antenna pair was positioned at the following heights: 48, 61, 71, 91, and 119 cm. Antenna separation distance for these heights was set to 64, 74, 89, 99, and 145 cm. The target was parametrized to match a plastic cylinder with a diameter of 20.5 cm and a height of 5.8 cm. Dielectric constants for the plastic cylinder, sand, and air were set to 3.27, 3.12, and 1, respectively.

3.2 Simulation of Antenna Height

In each gprMax height simulation, 121 A-scans were produced. Figure 3(a) shows the amplitude of the direct coupling between the transmitting and receiving antennae, as well as the amplitude of the S_2 reflection signal from the sand surface. Direct coupling characterizes the power coupling between the transmitter antenna and receiver antenna. gprMax considers antennae to be isotropic radiators, which provide no direction-dependent signal gain. However, each of the two horn antennae used later in the laboratory tests provides frequency-dependent directional gain between 5 and 11 dB. Typical directional gain for these antennae is estimated to be equal to 8 dB for each antenna or 16 dB total. Figure 3(a) also shows " S_2 reflection with antenna gain," which is the result of applying 16 dB of antenna gain to the raw reflection data.

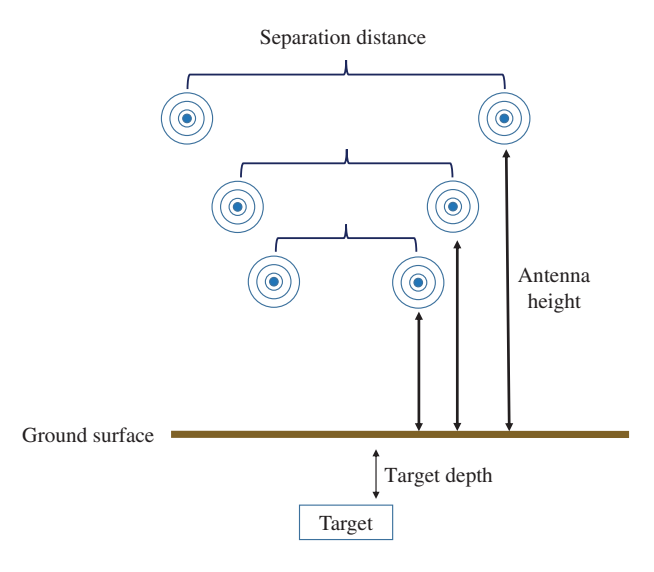


Fig. 2 Diagram of antenna heights.

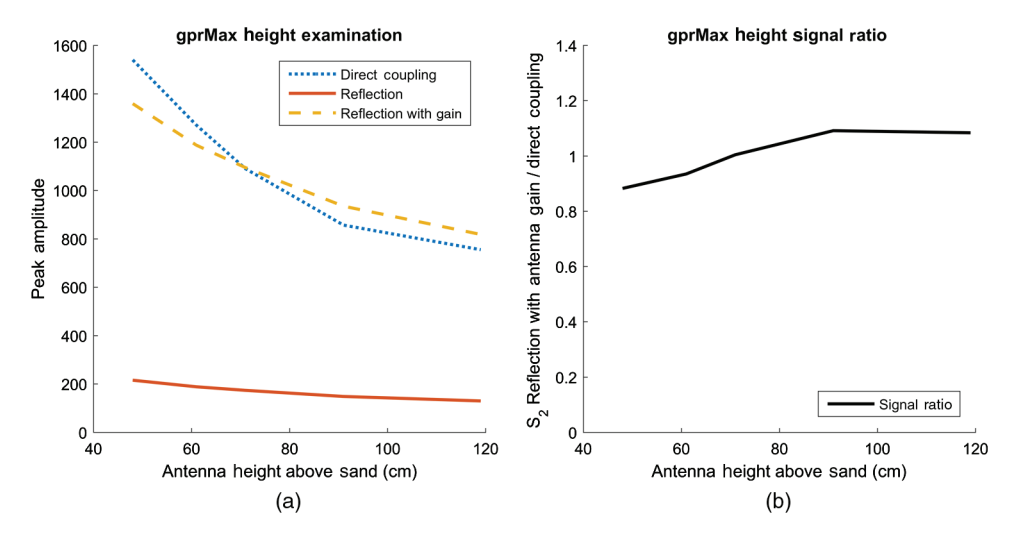


Fig. 3 Antenna height simulation results: (a) signal strengths and (b) the ratio of the signal strength of the reflected signal compared to the signal strength of the direct coupling.

Figure 3(b) shows the ratio of the reflection amplitude (with the applied antenna gain) to the direct coupling amplitude for each antenna height. The greater this ratio, the better GPR can detect a reflection—in this case the sand surface. Performance increases up to the 91-cm height, and then levels off, which indicates an optimal antenna height to be near 91 cm.

4 Experimental Study

4.1 Experimental Setup

A laboratory experiment was set up to examine the impact of antenna height and angle on GPR performance. A Keysight N9917A FieldFox handheld microwave analyzer (30 kHz to 18 GHz) was employed for radar signal transmission and detection. Figure 4(a) shows the plastic cylinder, which is used as the test target. It has a diameter of 20.5 cm, height of 5.8 cm, and dielectric constant of 3.27. Dielectric constants for the plastic cylinder and sand were calculated using surface reflectivity measurements taken in a frequency sweep from 30 KHz to 18 GHz. Figure 4(b) shows the radar testbed: a three squared meters wooden sandbox and scaffolding, Keysight N9917A, and two horn antennae. Sand was filled to a depth of 19 cm. Data were collected as both antennae were moved simultaneously across the sandbox.

The antennae were a pair of GIMA ultrawide-bandwidth horn antennae, 20 with operating bandwidth from 600 MHz to 6 GHz. The 3-dB beam bandwidth is approximately -25 deg to

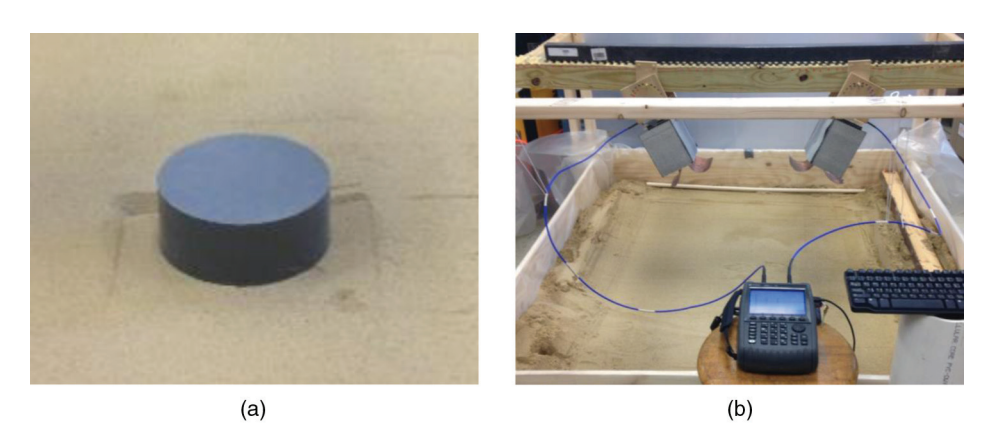


Fig. 4 Sandbox experimental test setup: (a) photograph of plastic cylinder target set on sand surface and (b) photograph of radar testbed with test configuration ($\Theta = 60$ deg, 61 cm antenna height) with two GIMA horn antennae.

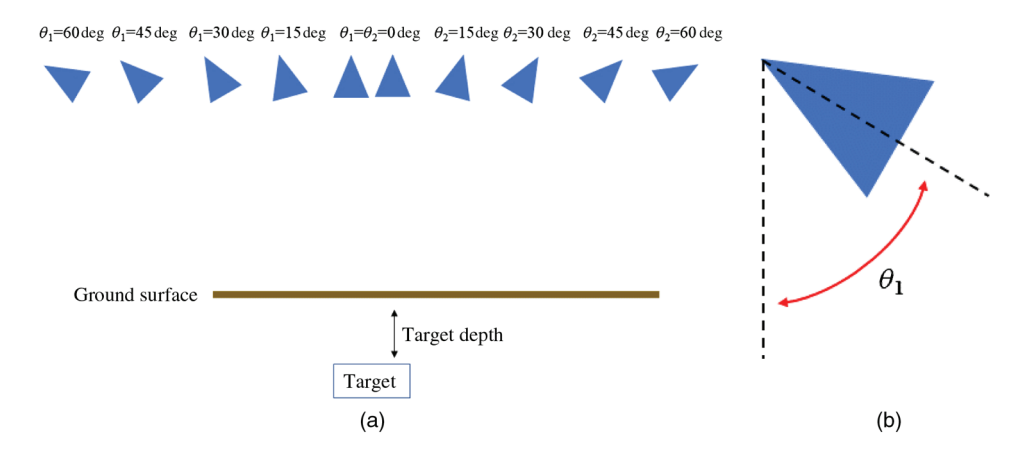


Fig. 5 (a) Diagram of antenna angles and (b) antenna angle measurement.

25 deg.²⁰ This directionality causes the elevation angle between a target and a horn antenna's main beam to have a significant impact on GPR image quality.²⁰ Antenna elevation angles are shown in Fig. 5(a). The angle of the transmitter is measured counterclockwise (θ_1), and the angle of the receiver is measured clockwise (θ_2), with respect to the downward pointing vertical axis. This is shown in Fig. 5(b). The antenna angle, Θ , is the sum: $\Theta = \theta_1 + \theta_2$. For example, if both transmitter antenna and receiver antenna have an angle of 45 deg, it results in $\Theta = 90$ deg.

4.2 Antenna Height Experiment

The antenna standoff heights and separations used in gprMax simulations were repeated in the sandbox testbed. For all heights tested, both the transmitter and receiver antennae were aligned with laser pointers to an inclination of 30 deg, for a total $\Theta=60$ deg. The plastic target was buried at a depth of ~8 cm, and the sand surface was raked smooth. At each of the five heights, 38 A-scans were taken at 2.54 cm intervals. For each A-scan, the average values of the antenna direct coupling signal, as well as the sand surface reflection signal (S_2) , were characterized and plotted in Fig. 6(a). Figure 6(b) shows the ratio of S_2 reflection amplitude to the direct coupling amplitude for each antenna height. The measurements show that the ratio increases up to the 71-cm height, and then decreases slightly, implying that optimal antenna heights are approximately between 71 and 119 cm, which is consistent with the gprMax simulation result of 91 cm. Because the testbed was only capable of specific antenna heights, the single best height, 71 cm, was chosen for subsequent testing.

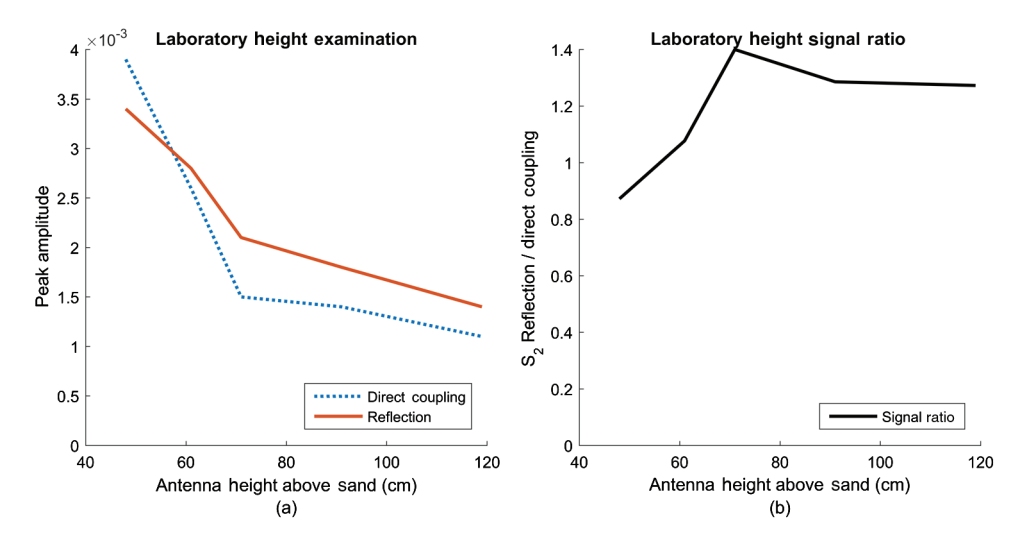


Fig. 6 Antenna height laboratory test results: (a) signal strengths and (b) the ratio of the signal strength of the reflected signal compared to the signal strength of the direct coupling.

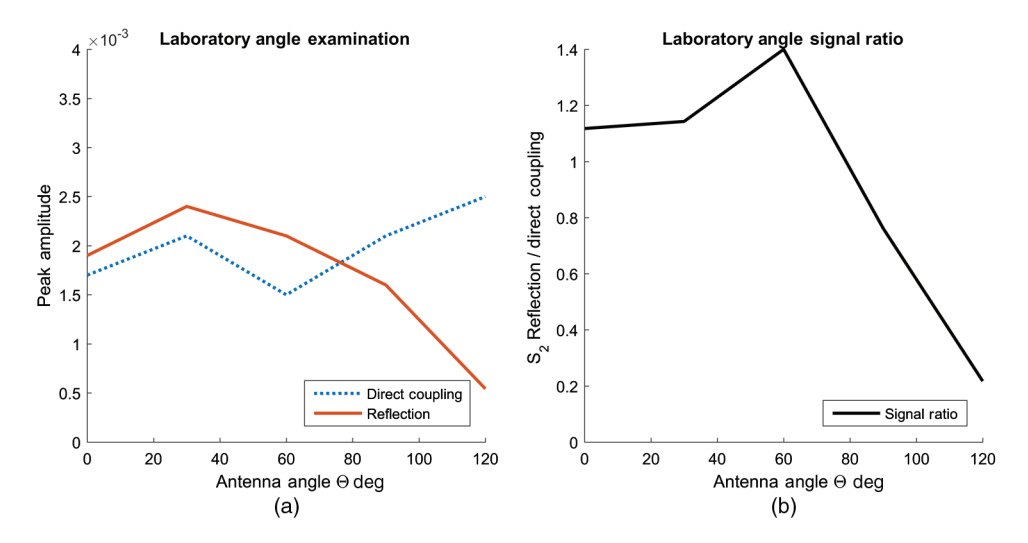


Fig. 7 Antenna angle laboratory test results: (a) signal strengths and (b) the ratio of the signal strength of the reflected signal compared to the signal strength of the direct coupling.

4.3 Antenna Angle Experiment

Tests were conducted to examine the effect of antenna angle on GPR performance. The antenna standoff height 71 cm was chosen based on the results of the antenna height examination. Five angle combinations were tested. Transmitter and receiver antennae were both set at 0 deg, 15 deg, 30 deg, 45 deg, and 60 deg, corresponding to an overall antenna angle of $\Theta = 0$ deg, 30 deg, 60 deg, 90 deg, and 120 deg, respectively. The target remained buried at a depth of 8 cm. At each angle, 38 A-scans were taken, 2.54 cm apart, as the antennae were moved together across the sandbox testbed. For each A-scan, the amplitude of the direct coupling between the antennae, as well as the reflected signal amplitude from the sand surface (S_2), were measured, as shown in Fig. 7(a). Figure 7(b) shows the ratio of the reflection amplitude to the direct coupling amplitude for each of the five tested antenna angles. The analysis indicates that a combined antenna angle of $\Theta = 60$ deg produced the highest ratio (1.4) of reflection amplitude.

5 Summation of Results

The calculated signal ratios for simulations and laboratory tests are plotted in Fig. 8. In the gprMax simulations shown in Fig. 8(a), variation of antenna height causes an 11.4% increase

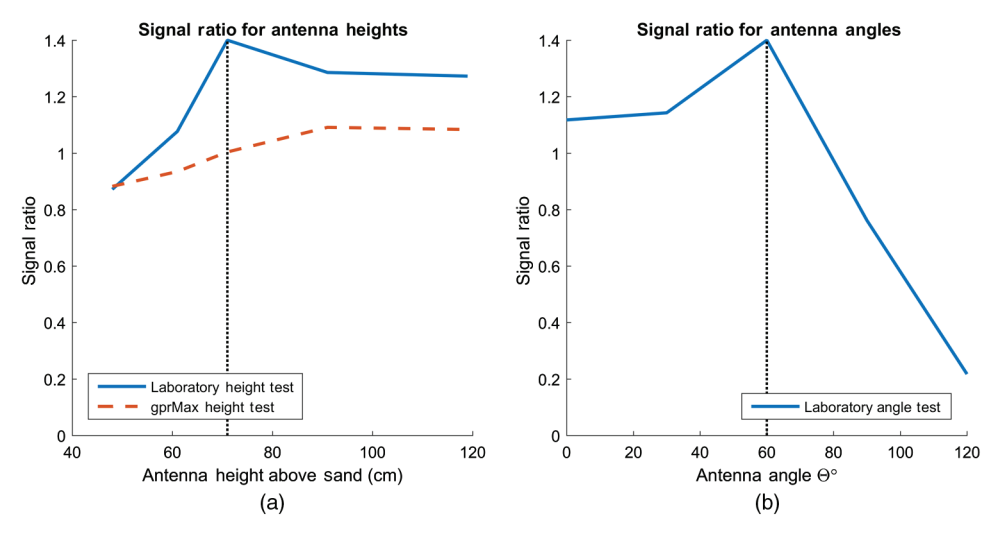


Fig. 8 Signal ratios as determined by gprMax and Laboratory Testing. A higher signal ratio indicates higher-quality data.

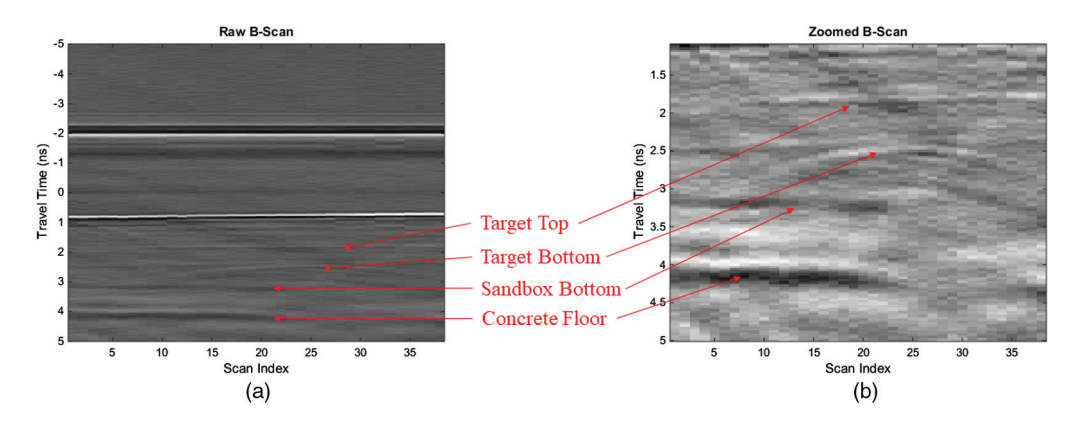


Fig. 9 (a) Unprocessed B-scan of sandbox containing gray target taken using antenna configuration with antenna height at 71 cm and antenna angle $\Theta=60\,$ deg. (b) A close-up view of the area-of-interest around the target.

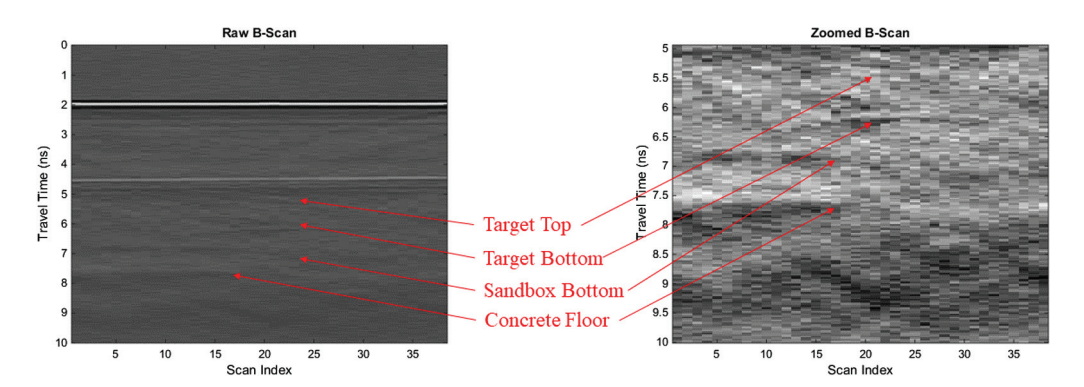


Fig. 10 Example of poor system performance: antenna height at 71 cm and antenna angle $\Theta = 120$ deg. (a) Unprocessed B-scan of sandbox containing grey target. (b) A close-up view of the target.

in signal amplitude as the antenna mounting height changes from 48 to 91 cm. Variations in antenna height during laboratory testing yield a 27.4% improvement when changing from 48 to 71 cm. Figure 8(b) shows that a 254% increase in signal ratio was observed between the worst-performing antenna angle ($\Theta = 120$ deg), and the best-performing antenna angle ($\Theta = 60$ deg).

Highest system performance occurred at an antenna height of 71 cm and an antenna angle of $\Theta = 60$ deg. These values are shown in Fig. 8 by vertical dotted lines. Figure 9 shows a B-scan image of the target taken by utilizing this antenna configuration.

For comparison, Fig. 10 shows a configuration that resulted in low system performance: 71-cm antenna height and $\Theta = 120\,$ deg. Notice the decreased visibility of the target features in both the raw and zoomed B-scans.

6 Discussion and Future Work

Antenna configurations featuring various antenna height and angle combinations have been examined. The laboratory tests and computer simulations conducted offer guidance for the design and capabilities of UAV-mounted air-launched GPR systems to be used for the detection of buried nonmetallic objects. This study found that for a bistatic GPR, the highest-quality data were obtained using an antenna height of 71 cm, and an antenna angle of $\Theta = 60$ deg. In laboratory testing, the 71-cm antenna height provided a signal ratio improvement of 27.4%, and the antenna angle $\Theta = 60$ deg provided a signal ratio improvement of up to 254%. By using the general parameters of surface reflectivity (S_2) and signal ratio, the results presented might be applicable to other GPR sensing applications beyond the detection of shallow-buried nonmetallic

targets. Further applications may include the GPR survey of bridge-decks⁴ and mapping of underground infrastructure.²¹ Additional research may serve to refine and expand these results, providing the groundwork for the design of next-generation UAV-mounted GPR systems.

Disclosures

The authors declare that this research was conducted in the absence of any business or financial relationships that could be construed as a conflict of interest.

Acknowledgments

This research was supported in part by U.S. National Science Foundation Grant Nos. 1647095 and 1640687, U.S. Army Contract/Grant No. W911NF-13-1-0301, and Office of Naval Research Grant No. N00014-16-1-2981. Some of this work has been previously published in "Zhang, Y. et al., buried nonmetallic object detection using bistatic ground penetrating radar with variable antenna elevation angle and height, in SPIE 10169, Nondestructive Characterization and Monitoring of Advanced Materials, Aerospace, and Civil Infrastructure 2017, 1016908."

References

- 1. K. C. Ho and P. D. Gader, "A linear prediction land mine detection algorithm for hand held ground penetrating radar," *IEEE Trans. Geosci. Remote Sens.* **40**(6), 1374–1384 (2002).
- 2. T. P. Montoya, "Land mine detection using a ground-penetrating radar based on resistively loaded Vee dipoles," *IEEE Trans. Antennas Propag.* **47**(12), 1795–1806 (1999).
- 3. H. M. Jol, *Ground Penetrating Radar Theory and Applications*, Elsevier, Amsterdam (2008).
- 4. X. Xu et al., "The development of a high speed ultrawideband ground penetrating radar for rebar detection," *ASCE J. Eng. Mech.* **139**(3), 272–285 (2013).
- 5. D. Huston et al., "GIMA ground penetrating radar system for monitoring concrete bridge decks," *J. Appl. Geophys.* **43**, 139–146 (2000).
- 6. Y. Zhang et al., "Advanced signal processing method for ground penetrating radar feature detection and enhancement," *Proc. SPIE* **9063**, 906314 (2014).
- 7. Y. Zhang et al., "2-D entropy and short-time Fourier transform to leverage GPR data analysis efficiency," *IEEE Trans. Instrum. Meas.* **64**(1), 103–111 (2015).
- 8. Y. Zhang et al., "Data analysis technique to leverage ground penetrating radar ballast inspection performance," in *IEEE Radar Conf.* (2014).
- 9. B. Sai, I. Morrow, and V. Genderen, "Limits of detection of buried landmines based on local echo contrasts," in *28th EuMc Workshop* (1998).
- 10. V. S. Chernyak, Fundamentals of Multisite Radar Systems: Multistatic Radars and Multistatic Radar Systems, 1st ed., p. 492, CRC Press, London (1998).
- 11. N. J. Willis, Bistatic Radar, Vol. 2, SciTech Publishing, Raleigh, North Carolina (2005).
- 12. T. Xia et al., "Performance enhanced high speed UWB GPR system for buried rebar detection," in *Symp. Appl. Geophys. Eng. and Environ. Prob.* (2013).
- 13. Y. Wang et al., "Adaptive imaging for forward-looking ground penetrating radar," *IEEE Trans. Aerosp. Electron. Syst.* **41**(3), 922–936 (2005).
- 14. W. Kang et al., "A study of antenna configuration for bistatic ground-penetrating radar," in *16th Int. Conf. Ground Penetrating Radar (GPR)*, pp. 1–4 (2016).
- 15. W. Kang et al., "The effect of the antenna height on quality of bistatic GPR data," in 9th Int. Workshop Adv. Ground Penetrating Radar (IWAGPR), Edinburgh (2017).
- R. Bloemenkamp and E. Slob, "The effect of the elevation of GPR antennas on data quality," in 2nd Int. Workshop Adv. Ground Penetrating Radar, Delft University of Technology, Delft, The Netherlands (2003).
- 17. D. Huston, *Structural Sensing, Health Monitoring, and Performance Evaluation*, Series in Sensors, B. Jones and W. B. Spillman, Eds., p. 645, Taylor and Francis, Burlington (2011).

- 18. C. Warren and A. Giannopoulos, "About the software," 2019, http://www.gprmax.com/about.shtml.
- 19. A. Ahmed, "Design and optimization of UWB antenna for air coupled GPR applications," Thesis, Electrical Engineering, University of Vermont, p. 61 (2014).
- 20. A. Ahmed et al., "Design of UWB antenna for air-coupled impulse ground-penetrating radar," *IEEE Geosci. Remote Sens. Lett.* **13**(1), 92–96 (2016).
- 21. D. Huston et al., "Urban underground infrastructure mapping and assessment," *Proc. SPIE* **10168**, 101680M (2017).

Daniel Orfeo received his BS degree in mathematics and a minor in physics from the University of Vermont (UVM) in 2014. In 2018, he received his MS degree in mechanical engineering from UVM with the thesis "Mechano-Magnetic Telemetry for Urban Infrastructure Monitoring." Currently, he is a doctoral candidate in mechanical engineering at UVM. His research interests include microwave and magnetic sensing and communications.

Yu Zhang received his BS degree from Huazhong University of Science and Technology, Wuhan, Hubei, China, in 2012 and his PhD degree from University of Vermont, Burlington, Vermont, United States, in 2017 both in electrical engineering. Since 2017, he has been a radar systems engineer at Aptiv, CA, USA, working on automotive radar for advanced driver assistance systems and autonomous driving vehicles. His general research interests include radar systems design and signal processing.

Dylan Burns attended the University of Vermont and in 2002 receiving his BS degree in mechanical engineering and minor in mathematics. He received his master's degree in 2006 in mechanical engineering, with his thesis research on "Aeroelastic Mechanics of Thin Films in Proximity Lithography." In 2011, he completed his PhD in mechanical engineering with his dissertation "Ambulatory Lordosimeter Measurement and Feedback Control of Seated Posture." Currently, he is a postdoctoral research associate.

Jonathan Miller is a senior engineer at White River Technologies. He obtained his BS degree in physics from Bates College and his MS degree in mechanical engineering from the University of Vermont. His research interests include application of magnetic and electromagnetic sensing to detection, subsurface characterization, and infrastructure monitoring. Currently, he is performing several projects involving integration of these sensor modalities with airborne and undersea platforms.

Dryver Huston is a professor of mechanical engineering at the University of Vermont. His research interests include sensing techniques for structural health monitoring and subsurface characterization. He has a PhD (1986) and MA (1982) from Princeton University, and his BS from the University of Pennsylvania (1980).

Tian Xia is a professor with the Department of Electrical and Biomedical Engineering at the University of Vermont. His research interest focuses on sensing circuit and system design and test. Recently he has been investigating nondestructive evaluation technology for the application of smart city underground utility inspection and mapping. He received IEEE Green Mountain Section "Leadership Award" in 2011 and IEEE Green Mountain Section "Faculty of the Year Award" in 2017.